Monodisperse Hexagonal Silver Nanoprisms: Synthesis *via* Thiolate-Protected Cluster Precursors and Chiral, Ligand-Imprinted Self-Assembly

Nicole Cathcart and Vladimir Kitaev*

Chemistry Department, Wilfrid Laurier University, 75 University Avenue West, Waterloo, Ontario, Canada N2L 3C5

ABSTRACT Silver nanoprisms of a predominantly hexagonal shape have been prepared using a ligand combination of a strongly binding thiol, captopril, and charge-stabilizing citrate together with hydrogen peroxide as an oxidative etching agent and a strong base that triggered nanoprism formation. The role of the reagents and their interplay in the nanoprism synthesis is discussed in detail. The beneficial role of chloride ions to attain a high degree of reproducibility and monodispersity of the nanoprisms is elucidated. Control over the nanoprism width, thickness, and, consequently, plasmon resonance in the system has been demonstrated. One of the crucial factors in the nanoprism synthesis was the slow, controlled aggregation of thiolate-stabilized silver nanoclusters as the intermediates. The resulting superior monodispersity (better than *ca.* 10% standard deviation in lateral size and *ca.* 15% standard deviation in thickness (<1 nm variation)) and charge stabilization of the produced silver nanoprisms enabled the exploration of the rich diversity of the self-assembled morphologies in the system. Regular columnar assemblies of the self-assembled nanoprisms spanning 2−3 μm in length have been observed. Notably, the helicity of the columnar phases was evident, which can be attributed to the chirality of the strongly binding thiol ligand. Finally, the enhancement of Raman scattering has been observed after oxidative removal of thiolate ligands from the AgNPR surface.

KEYWORDS: silver nanoparticles · prisms · platelets · silver clusters · self-assembly · chiral · helical · SERS

Metal nanoparticles have demonstrated their great utility in a variety of applications including plasmonics,[1] catalysis,[2] and sensing.[3] To fully implement the advantageous properties of metal nanoparticles, control over their size, shape, and assembly is necessary.[4] Silver is remarkably versatile in shape-controlled NP synthesis due to a relative ease of its oxidative etching.[5] In terms of optical applications, silver has the best plasmonic properties of all chemically stable metals. To attain a full spectral range of plasmonic resonances, anisotropic silver particles (AgNPs) have to be prepared.[4,6] For instance, small (up to *ca.* 20 nm) spherical silver particles have plasmon absorbance at *ca.* 400 nm, which red shifts slowly with the increase in sphere diameter and more significantly with increasing anisotropy and corner sharpness of AgNPs.[7] One of the earliest and most studied anisotropic AgNPs are prisms (platelets).[8,9] Silver nanoprisms (AgNPRs) have been prepared by a variety of approaches through thermal[10] and photochemical[11] routes using different capping ligands.[12] The variation of AgNPR dimensions (lateral size, thickness, and degree of truncation/snipping) has been demonstrated by different methods.[5,9] Several post-modification approaches to tune AgNPR dimensions and plasmonic properties have been reported.[13−16] At the same time, the reliable and reproducible synthesis of monodisperse silver nanoprisms remains to be a research in progress due to the kinetic nature of their formation[5,9] driven by the growth of planar twinned defects.[17,18] The monodispersity of AgNPRs remains a crucial factor for taking advantage of their wavelength-dependent plasmonic properties and realization of colloidal self-assembly.

Self-assembly of colloidal nanoparticles in concentrated dispersions or upon solvent evaporation from colloidal dispersions has recently attracted a growing interest.[19] From a perspective of fundamental understanding, organization of colloidal particles provides instructive modeling of molecular assemblies. Nanoparticle assemblies are also of interest due to their ability to tailor the collective properties of a NP ensemble.[20] Through NP self-assembly, a great diversity of complex and fascinating packing motifs can be realized.[21−23] In particular, mesoscopic ordered phases have been described, whereby

* Address correspondence to vkitaev@wlu.ca.

Received for review June 24, 2011 and accepted August 21, 2011.

Published online August 22, 2011
10.1021/nn2023478

the ordering and organization of anisotropic NPs is similar in many aspects to liquid crystals.[24−26] Packing of platelets and prisms in columnar assemblies, where prisms arrange together side-by-side,[27,28] closely resembles discotic liquid crystals. Such columnar packing maximally excludes solvent and minimizes the total entropy of the system.[29] The NP assembly is thus driven by the depletion forces in concentrated solutions and by capillary forces in drying dispersions.[30] Noteworthy, the use of discotic liquid crystalline molecules as capping agents has been explored for NP assembly.[31] Assembly of AgNPRs has been studied in terms of both their stacking[32] and monolayer properties.[33] Recently, more detailed studies of the silver nanoprism assemblies have been reported.[34] Packing of AgNPRs in columnar arrangements and the tendency of the nanoprisms to stack perpendicularly to the substrate regardless of the type of substrate have been described. The latter has been attributed to attractive forces between NP faces dominating over the forces between the nanoprisms and the substrate.[30] In most of the reported AgNPR assemblies, the prisms were appreciably polydisperse, which significantly hampered long-range ordering in their assemblies.

Herein, we describe a one-stage, aqueous room temperature procedure to produce monodisperse silver nanoprisms capped with the chiral thiol ligand, captopril, through the triggered aggregation of silver nanoclusters. The key principal feature of the reported synthesis is the formation of thiolate-stabilized clusters and their controlled aggregation into AgNPRs with very good monodispersity. These synthesized monodisperse AgNPRs feature tunable dimensions and plasmon absorbance, as well as display a rich variety of novel self-assembled structures including helical columnar morphologies induced by the chiral ligand.

RESULTS AND DISCUSSION

Key aspects of the AgNPR synthesis are summarized in Figure 1. The nanoprism formation is a complex process that can be subdivided into several stages (Figure 1a). The starting point is the reduction of silver nitrate in the presence of captopril and citrate as stabilizing ligands, leading to the formation of silver nanoclusters. These thiolate-protected nanoclusters are a mixture of reduced silver species mostly smaller than 2 nm, judging by their ultracentrifugation properties—no (or very little) sedimentation after 90 min at 50 000 rcf. Their formation is indicated by a characteristic UV−vis signature (spectrum ① in Figure 1b). TEM images of thiolate-protected nanoclusters (Figure S1 in the Supporting Information) further corroborate the presence of smaller particles, as well as show some aggregation to larger entities that likely took place upon drying. Compared to other nanoprism preparations with smaller silver intermediates,[10] the silver nanoclusters in the described synthesis remained stable and unchanged in an as-prepared state at least for several weeks due to strongly binding thiols, despite the presence of hydrogen peroxide and absence of stabilizing polymers, such as polyvinylpyrrolidone (PVP). We found that PVP was not required in the presence of thiols and was, in fact, detrimental to the formation of the thiolate-stabilized AgNPRs. The presence of PVP (at 1.0 mM total concentration in solution) slowed the nanoprism development, as reported,[5,10] and resulted in appreciably broader AgNPR size distribution in our synthesis conditions.

Nanocluster aggregation into nanoprisms could be triggered by a strong base, upon addition of which the prism formation process started within 5 to 20 s and proceeded to completion within several minutes, as could be observed by changes in UV−vis spectra (Figure 1b). Before the reduction, the mixture of captopril, silver nitrate, citrate, and hydrogen peroxide is transparent with no absorption in the visible range, and importantly, insoluble thiolates are not formed (spectrum ⓪ in Figure 1b). Upon reduction with borohydride, silver nanoclusters start to form, indicated by the emergence of a characteristic broad peak at *ca.* 420 nm (spectrum ① in Figure 1b). When potassium hydroxide was added, the nanocluster peak lost some but not all of its intensity and red-shifted (spectra ② to ④) before the emergence of the plasmonic peak corresponding to nanoprisms (spectrum ⑤). The plasmonic peak of the nanoprisms continued to develop within *ca.* 5 min (spectra ⑥ to ⑧), at which time the AgNPR development was complete. It is important to emphasize that the aggregation process does not occur without the addition of strong base, such as KOH. Without KOH, the crude clusters remain nonaggregated for as long as several months.

To further the point of the importance of cluster formation prior to aggregation to prisms, reduction of silver in the same conditions and reagent concentrations, with the thiol and borohydride combined separately and added last together, does not yield AgNPRs, as documented in Figure S2. Several samples have been prepared to emphasize this point, also varying the order of addition of citric acid, KOH, and KCl. All of these samples feature broad spectra that clearly point out that, without the formation of cluster precursors, no prisms will form. Thus, silver clusters and not silver ions or silver thiolates are a key precursor in the described AgNPR synthesis.

Synthesized AgNPRs have a hexagonal (or highly truncated triangular) prismatic shape (*e.g.*, Figure 6). The hexagonal shape is formed when all lateral directions along the planar twinning defects grow fast and uniformly upon cluster aggregation.[15] The fast growth of the AgNPs is a consequence of triggered cluster destabilization by a combination of base and citrate and cluster aggregation serving as a rate-limiting stage

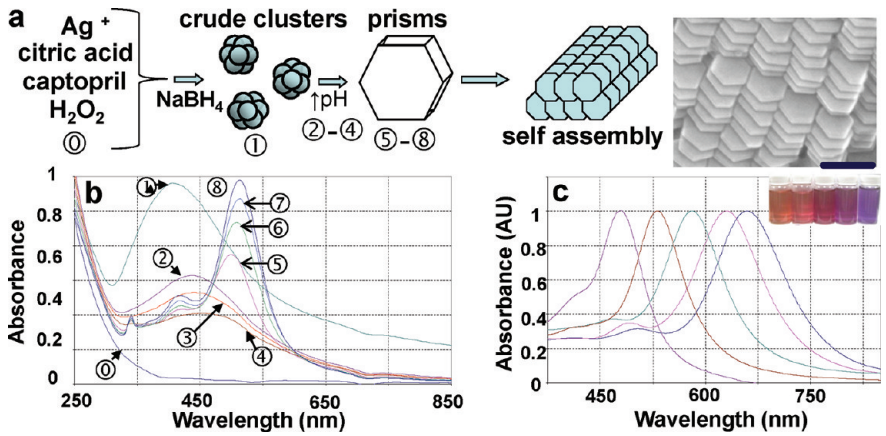

Figure 1. Summary of the formation process and main properties of AgNPRs: (a) schematic of the synthesis and self-assembly with the representative SEM image of self-assembled AgNPRs. Numbers are the formation stages. (b) UV−vis spectra of ⓪, solution before reduction; ① and ② solutions of crude nanoclusters immediately after reduction and directly after the addition of KOH; ③ and ④ onset of the aggregation of nanoclusters; ⑤ onset of AgNPR formation; ⑥−⑧ growth of the nanoprisms to their final size. (c) Normalized UV−vis spectra of several synthesized AgNPRs with optical photographs of representative AgNPRs dispersions in the inset. Scale bar is 100 nm.

in the AgNPR formation process. Deviations from the hexagonal shape toward the truncated triangular morphologies have been typically observed for slower than normal growth due to different synthetic factors.

The produced AgNPRs are stable for at least several months; both plasmonic peaks and electron microscopy images remain unchanged. The onset of the nanoprism formation could be readily observed by the bicolored appearance of the samples due to both scattering and plasmonic absorbance of large silver nanoparticles.[35] The scattering appeared first at the top of the reaction media, which was exposed to atmospheric oxygen—that corroborates aggregation driven by oxidative processes.[8,10] The main oxidizing reagent in the reported AgNPR synthesis is hydrogen peroxide. In absence of hydrogen peroxide, some nanocluster aggregation takes place but leads to ill-defined aggregates with characteristic popcorn shapes (Figure S3). Presence of citrate as a reducing and stabilizing agent is also crucial for silver prism formation. In the absence of citrate, clusters do not aggregate upon base addition, as shown in Figure S4b. At low citrate concentrations, limited cluster aggregation led to poorly defined nanoparticles with multiple defects (Figure S4c).

In addition to the essential reagents described above, chloride has been found to be beneficial (but not absolutely required) for the formation of well-defined AgNPRs with good monodispersity (see Table 1). Such monodisperse nanoprisms self-assemble readily, as shown in the right panel of Figure 1a. By variation of the synthetic conditions, both the thickness and the width of AgNPRs can be tuned, and hence the optical properties of the dispersions, as illustrated in Figure 1c by the variation in plasmon absorption spectra and optical photographs of the vials. The detailed role of the reagents in AgNPR synthesis (captopril, citrate, sodium borohydride, hydrogen peroxide, potassium hydroxide, and potassium chloride) and their interplay is described below.

Role of the Reagents in the Synthesis of Thiolate-Stabilized AgNPRs. We first discuss the effect of the variation of one of the reagent concentrations. For minimizing the complexity of the interplay of chloride with other reagents, chloride has not been used for the series of samples described in Figure 2a−c. The concentrations of other reagents (not being varied) have been kept constant at 2.7 mM citric acid, 0.37 mM captopril, 0.67 mM $AgNO_3$, 13.3 mM H_2O_2, 4.3 mM $NaBH_4$, and 10.1 mM KOH.

Citrate is a commonly used charge stabilizing agent for AgNPs in aqueous solutions.[35] In the reported synthesis, the stabilizing role of the citrate for the formed AgNPR may be secondary compared to that of a strongly binding water-soluble thiol, captopril, that was also used. At the same time, the citrate plays a key role in AgNPR formation. At low citrate concentrations, under 1.15 mM, the silver nanoclusters do not aggregate into larger prisms upon the base addition. In the absence of citrate, smaller NPs remain stable (Figure S4b), while at citrate concentrations lower than optimal, clusters aggregate partially into ill-defined nanoparticles (Figure S4c). It seems that citrate is needed as a reducing agent for the silver ions that are present in thiolate cluster shells[36] and have to be converted to metallic silver for AgNPRs. Second, complexation of silver in solution and stabilization of (111) planes upon prism growth are other important functions of the citrate, and borohydride (as another reducing agent) is not able to replace citrate. At higher citrate concentrations (above *ca.* 3.1 mM), the crude nanoclusters aggregated into polydisperse nanoparticles (yellow solutions with broad absorbance spectra). Variation of the citrate concentrations in the range from 1.15 to 3.1 mM

TABLE 1. Synthesis Conditions Describing the Preparation of AgNPR Samples That Displayed Best Monodispersity and Highly Ordered Self-Assembled Structures

citric acid (mM)	captopril (mM)	silver nitrate (mM)	hydrogen peroxide (mM)	KCl (mM)	sodium borohydride (mM)	KOH (mM)	Plasmon λ_{max} (nm)	corresponding figure(s) of EM images
0.78	0.26	0.49	9.73	0.34	2.34	6.81	555	8a
0.77	0.35	0.48	9.63	0.34	2.31	7.32	531	13
0.77	0.38	0.48	9.62	0.34	2.31	7.31	613	9c,d
0.94	0.32	0.59	11.80	0.12	2.83	16.52	526	12e
0.83	0.28	0.52	10.34	0.29	2.48	7.86	544	9a,b
0.83	0.28	0.52	10.34	0.29	2.48	7.86	544	10c,d, 11b
0.81	0.27	0.51	10.17	0.31	2.44	7.73	559	11c, 12b,d
0.81	0.27	0.51	10.17	0.31	2.44	7.73	559	10a
0.75	0.25	0.47	9.40	0.24	2.26	7.14	553	12c
0.77	0.26	0.48	9.68	0.34	2.32	7.35	558	10b
2.69	0.36	0.67	13.70	0.00	3.22	10.21	543	12f
2.69	0.36	0.67	13.70	0.00	3.22	10.21	543	8d

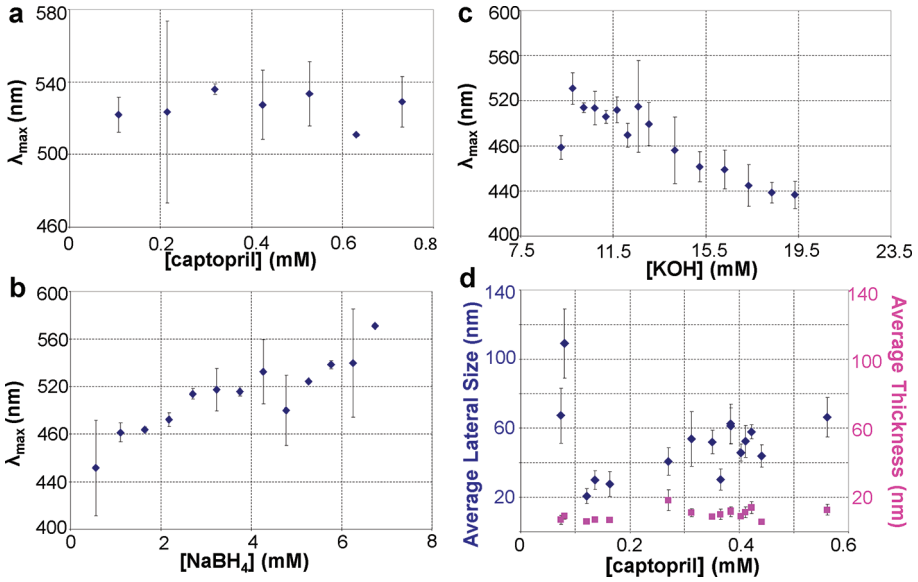

Figure 2. Role and effect of different reagents on AgNPR synthesis. Dependence of the resulting λ_{max} of AgNPR plasmon absorbance on concentrations of (a) captopril; (b) sodium borohydride; and (c) potassium hydroxide. Representative EM images of AgNPRs for the boundaries of the ranges at each plot are given in Figure S5. Note that these samples series described in (a−c) have been prepared in the absence of chloride to minimize complexity. (d) Overall relationship between captopril concentration and both lateral size (blue points) and thickness (magenta points) of AgNPRs for various series of samples (measured by EM) with and without chloride and varying concentrations of other reagents. Note that the observed variations in size are largely due to the interplay of chloride and captopril (in contrast to panel a).

did not exert significant influence on plasmon absorbance, thickness, or lateral size of the resulting AgNPRs.

Captopril ((2*S*)-1-[(2*S*)-2-methyl-3-sulfanylpropanoyl]-pyrrolidine-2-carboxylic acid) is a strongly binding water-soluble ligand that plays the major role in the formation of crude nanocluster intermediates. The minimum concentration of captopril required for thick AgNPR formation is *ca.* 0.05 mM. Below this concentration, nanoclusters were not stabilized and uncontrolled aggregation occurred before KOH addition. Captopril concentration had a relatively low effect on the AgNPR dimensions and the wavelength of maximum absorbance (λ_{max}), which is demonstrated in Figure 2a. A stronger captopril effect has been observed at its lower concentrations between 0.15 and 0.25 mM, where the peak of maximum absorbance could change by *ca.* 50 nm. Above 0.62 mM captopril, nanoclusters did not convert to nanoprisms. At larger concentrations (>0.2 mM), captopril also suppressed the effect of other reagents, as shown in Figure 2d for overall data on AgNPR produced using different chloride concentrations. When captopril concentrations were low (between 0.05 and 0.1 mM), the largest AgNPRs (65−110 nm) could be produced by varying chloride; at moderate captopril concentrations (0.1−0.4 mM), AgNPRs with lateral size between 20 and 60 nm could be produced; while at higher captopril concentrations (0.4−0.62 mM), AgNPR lateral dimensions remained relatively constant in a range between 40 and 65 nm. In terms of nanoprism thicknesses, captopril had an insignificant effect. The

observed effect of captopril in AgNPR synthesis can be rationalized in terms of it being a strongly binding ligand in an appreciable excess to the amount sufficient for surface stabilization of larger AgNPRs. Finally, we have tested another water-soluble thiol, glutathione, in AgNPR synthesis. In the same conditions, the silver nanoclusters stabilized with glutathione did not aggregate, which did not allow producing AgNPRs. The resistance to aggregation of glutathione-protected clusters is likely due to a larger size of the glutathione and its better steric protection compared to captopril.

Sodium borohydride served as a reducing agent. Similar to other reported syntheses of silver nanoprisms,[10] with the increase in borohydride concentration, AgNPR lateral size became larger, as can be deduced from the dependence of the plasmon maxima, shown in Figure 2b and confirmed by electron microscopy (Figure S5). Minimum sodium borohydride concentration of 0.55 mM was required to form the nanoclusters that were capable of transformation to nanoprisms. Under this borohydride concentration, the crude clusters are not stable enough to undergo aggregation, and the solution clears, signifying the oxidation of silver to an ionic form. Above 6.7 mM sodium borohydride, the nanoclusters remained largely intact (Figure S4a); that is, they did not aggregate to nanoprisms upon addition of sodium hydroxide within a long period of time (hours to days) and subsequently (upon ultimate decomposition of the borohydride excess) produced AgNPRs with poor size distribution and large amounts of irregular aggregates. Higher borohydride concentration likely suppresses oxidative etching of silver clusters (by providing extra electrons)[37] that is essential to cluster coalescence into nanoparticles. Together with the data of Figure S2, it emphasizes the point that cluster destabilization and aggregation is the key step in AgNPR formation and is the kinetically slowest one. Thus protecting the cluster from aggregation results in the lower effective concentration of nucleating species and correspondingly lower supersaturation and the lower number of AgNPR seeds formed. The smaller amount of seeds results in larger final AgNPRs. The observation of the increasing prism edge length with increasing borohydride concentration is also consistent with the reported findings for the synthesis of silver prisms based on oxidative etching.[10]

Hydrogen peroxide has been documented to function as a key reagent that triggers AgNPR formation out of freshly reduced silver nanoclusters/nanoparticles.[10,38] Peroxide plays a central role in the destabilization of the nanoclusters and promotion of their selective aggregation coupled with shape selection through the oxidative etching of silver.[5] In our synthesis, lower peroxide concentrations yielded polydisperse populations of nanoprisms as well as shapeless aggregates reminiscent of popcorns (Figure S3). The low critical concentration of peroxide for cluster aggregation was 4.2 mM. Below 4.2 mM, the crude nanoclusters did not aggregate to form nanoprisms. In the range from 4.2 to *ca.* 12 mM of peroxide, the development of AgNPRs required significantly longer times (10 min *vs* typical <1 min) and the nanoprisms were more prone to subsequent degradation, which was evident by the increasing proportion of popcorn morphologies, etched AgNPRs, and the colloidal collapse of the system. The optimal concentration of peroxide has been found to be *ca.* 13.5 mM, which produced AgNPRs with the highest shape selection (>98%) and optimal monodispersity and hence superior optical properties. This optimal peroxide concentration is near the limit, above which (*ca.* 15 mM) all AgNPs completely dissolve due to oxidation.

Potassium hydroxide has been used in the reported synthesis to promote aggregation of the nanoclusters into nanoprisms. (NaOH has often been used instead of KOH with the same results.) Initially, upon reduction with borohydride, the solution became pale yellow to light orange/brown, at which point KOH was added all at once. After KOH addition, the cluster solutions became lighter and then progressed changing through different colors (yellow to orange to red to purple to blue for largest samples), while increasing in absorbance intensity indicated growth of AgNPRs. The minimum concentration of KOH that triggered the nanoprism formation was 8.1 mM with the corresponding solution pH of *ca.* 9.1. The largest AgNPRs were produced in a range of KOH concentrations between 9 and 11 mM (pH = 9.2−10.5) (Figure 2c), with AgNPRs getting smaller at higher KOH concentrations. At KOH concentrations higher than 18 mM (pH > 12), the decrease in AgNPR size leveled off (Figure 2c). A proposed explanation for the role of the strong base in triggering cluster aggregation is the thiolate disruption due to the competitive coordination of hydroxide ion to silver. Citrate likely assists in thiolate destabilization both by coordinating to silver and as a reducing agent to reduce the silver form a thiolate shell to the metallic silver. Disruption of the thiolate shell should cause coalescence of highly energetic (relative to nanoparticles and bulk phase) clusters to AgNPRs. In this scenario, observed formation of smaller prisms at high KOH concentration is accounted for by stronger disruption of the clusters that triggers faster nucleation with more nuclei and consequently prisms growing to smaller sizes.

Chloride ions have been found to serve as an effective additive for the size control of the AgNPR synthesis.[38] Chloride ions were not essential for AgNPR formation (in contrast to all other reagents) but have been realized to be beneficial in terms of synthesis reproducibility, AgNPR monodispersity, and, consequently, self-assembly. Chloride ions also had a strong effect on the thickness of these nanoprisms, with the observed maximum of AgNPR thickness reached at intermediate chloride concentrations. The relationship between chloride concentration and AgNPR thickness is shown in Figure S6, which also displays SEM and TEM

TABLE 2. Summary of the Role of Reagents, Their Effect, and Optimal Concentration in AgNPR Synthesis

	concentration (mM) without/with KCl			
reagent	lowest	optimal	highest	role in the synthesis and major effect on plasmon absorption wavelength (PLAW), size, thickness, and monodispersity of AgNPRs
citric acid	1.15/0.67	2.7/0.77	3.1/1.4	needed for cluster conversion and AgNPR costabilization; no significant influence on PLAW, thickness, or lateral size
captopril	0.05/0.14	0.37/0.26	0.62/1.2	required for cluster formation; minor influence on PLAW and thickness; largest lateral sizes were achieved with chloride at captopril concentrations in a range of 0.05−0.1 mM, above which smaller AgNPRs were formed
sodium borohydride	0.55/2.1	4.3/2.3	6.7/3.1	required for silver reduction and cluster formation; upon increase in borohydride concentration, lateral size and PLAW increased
hydrogen peroxide	4.2/2.9	13.3/9.7	15.0/38.7	needed for oxidative etching of AgNPRs and cluster conversion — lower peroxide concentration resulted in high polydispersity; no direct effect on PLAW, size, and thickness
potassium hydroxide	8.1/5.8	10.1/7.4	>18/>77	major reagent for cluster conversion to AgNPRs; upon increase in KOH concentration, PLAW and size decreased
potassium chloride	——/0	——/0.34	——/0.34	not essential, but improves AgNPR monodispersity; highest AgNPR thicknesses were achievable at 0.15 mM KCl, above which thickness reduced; largely no effect on PLAW or size

images of representative samples. Error bars in the figure are the standard deviations of measurements from a single sample averaged at least for 50 particles, while several samples have been prepared to ensure reproducibility and reliability of the reported data. Starting with no chloride, the AgNPR average thickness was 10.1 ± 1.5 nm, the nanoprism polydispersity was high, and AgNPR ordering was low (Figure S6a). At the range of chloride concentrations from 0.02 to 0.13 mM, the AgNPR thickness increased from *ca.* 9 to 18 nm, with the maximum thickness in a system observed at *ca.* 0.13 mM of chloride. In this range, AgNPR monodispersity has been improved, resulting in better ordering upon self-assembly, as can be seen in Figure S6b,c (0.02 and 0.13 mM chloride, respectively). At chloride concentrations higher than *ca.* 0.15 nm, the AgNPR thickness reduced from *ca.* 18 nm to between 5 and 10 nm and remained fairly constant. Figure S6d shows AgNPRs prepared with the highest amount of chloride (0.31 mM) which have comparable thicknesses (6.2 ± 0.9 nm) to the AgNPRs shown in Figure S6c. Chloride had a competing effect with thiols since both of them bind strongly to AgNPR surface. Correspondingly, higher thiol concentrations suppressed the effect of chloride. The effect of chloride on thickness became moot at higher captopril concentrations of *ca.* 0.35 mM, while an effect of chloride on AgNPR width was most evident at low thiol concentrations (<0.2 mM).

The summary of the main role of the reagents in the AgNPR synthesis and their optimal concentrations are given in Table 2.

Interplay of Reagents in AgNPR Synthesis. The first observation of the reagent interplay is the effect of chloride in conjunction with the citrate. It has been observed that, when using chloride, the citrate concentration had to be lowered to 0.77 mM to produce high-quality AgNPRs. Citrate serves as a complexing agent for silver and likely competed with the chloride binding to the silver surface and the formation of insoluble silver chloride. Consequently, higher citrate concentrations suppressed the beneficial role of chloride for the AgNPR shape selectivity and monodispersity.

More involved and central to the successful AgNPR preparation was the interplay of KOH and KCl. In general, for higher chloride concentrations, lower KOH concentrations were required to produce monodisperse AgNPRs. For instance, at high chloride concentrations (>0.35 mM), concentrations of KOH greater than 8.3 mM were needed to yield monodisperse AgNPRs with sharp plasmonic peaks. At chloride concentration in a range from 0.27 to 0.35 mM, 11 mM KOH has been found to produce optimal AgNPRs. For chloride concentrations between 0.13 and 0.27 mM, the minimum concentration of KOH to produce optimal particles was 8.4 mM. Lower concentrations of KCl (between 0.09 and 0.13 mM) produced AgNPRs with broad plasmon absorption spectra, indicative of polydispersity. Under the KCl concentration of 0.07 mM, when the citrate concentration was below *ca.* 0.8 mM, nanoprisms could not form. At higher citrate concentrations of 3.0 mM, chloride was not necessary for stabilization of AgNPRs and actually had a detrimental

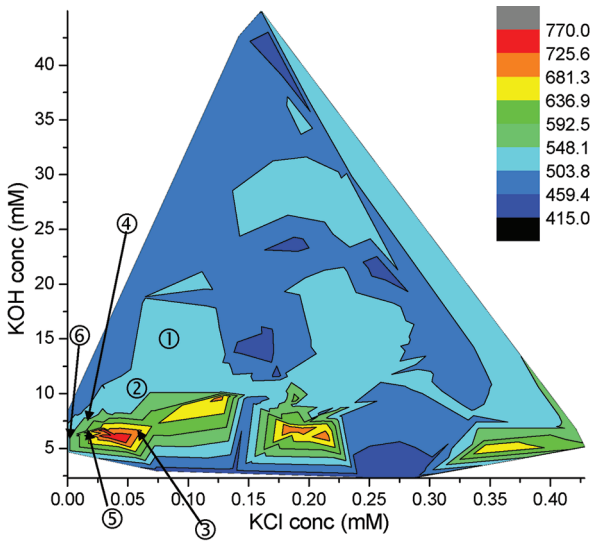

Sample	λ_{max}(nm)	KCl (mM)	KOH (mM)	HWHM (nm)	% Packing
①	520	0.11	16.5	53	85
②	551	0.07	10	53	75
③	632	0.07	7.1	104	50
④	637	0.02	7.2	115	85
⑤	753	0.02	6.7	141	85
⑥	517	0	6.2	67	95

Figure 3. Contour plot of the maxima of the plasmon resonance, λ_{max}, of the synthesized AgNPRs as a function of concentrations of potassium hydroxide and potassium chloride. For the selected AgNPR samples of the most interest, the data on concentrations of KCl and KOH, sharpness of plasmonic peak at λ_{max} measured from UV−vis spectra and expressed as the peak half-width at half-maxima (HWHM), and tentative indications of % of highly ordered packing assemblies are summarized in the adjacent table.

effect starting from 0.3 mM. Figure 3 displays the relationship between chloride and hydroxide concentrations in the synthesis and the maximum plasmon absorbance of the resulting AgNPRs. It corroborates the discussed correlation of KOH and chloride concentrations and also shows that lower KOH concentrations resulted in plasmon absorbance at larger wavelengths and hence nanoprisms with larger lateral dimensions, while higher KOH concentrations yielded smaller AgNPRs. When considered in combination with KOH, chloride did not appear to have a significant influence on AgNPR plasmon absorbance and width.

Overall, chloride was found to have a beneficial effect on the reproducibility of the synthesis and AgNPR monodispersity, which can be attributed both to the etching of less stable nanoparticles and binding to the surface of AgNPRs during nanocluster aggregation. As can be seen in Figure 3, the largest nanoprisms have been produced at *ca.* 5 mM of KOH in a wide range of chloride concentrations. Samples ①, ④, ⑤, and ⑥, can be considered to be the most monodisperse AgNPRs, judging by the plasmonic peak width, and have been produced with (samples ①, ④, and ⑤) and without chloride (sample ⑥). On the basis of the greater percentage of the samples with chloride having narrower peaks of plasmonic absorbance and consequently higher monodispersity confirmed by electron microscopy, the addition of chloride greatly helps to improve reproducibility of the synthesis, AgNPR monodispersity, and packing, as has been observed by EM imaging.

Attaining synthesis reproducibility and, most importantly, AgNPR monodispersity has been crucial for the realization of the highly ordered structures upon nanoprism self-assembly. The combination of high hydroxide concentrations at higher concentrations of chloride resulted in the best quality of self-assembly, in terms of the long-range order and diversity of structures. For the combination of either low chloride and high hydroxide or high chloride and low hydroxide concentrations, the AgNPR self-assembly was relatively poor. The dominant observed trend was that when the ratio of concentrations of potassium hydroxide to potassium chloride was greater than 150:1; the self-assembly has been appreciably better than when this ratio was lower. It follows that, when both chloride and hydroxide concentrations were low, the self-assembly improved, as long as KOH/KCl ratio >150 was still maintained.

Self-Assembly of Monodisperse AgNPRs. *General Considerations.* The synthesized AgNPRs featured aspect ratios (width-to-thickness) varying from 4 to *ca.* 20, with the majority of samples in a range from 5 to 10.

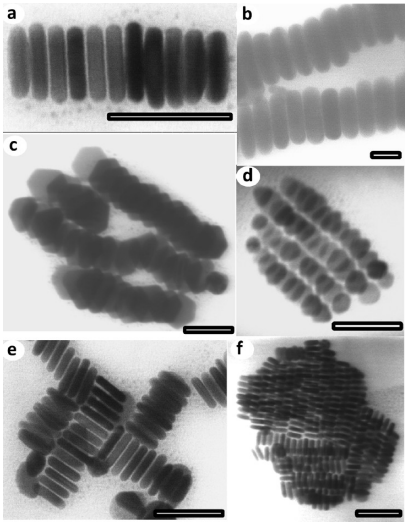

Figure 4. TEM images of parallel stacking of silver nanoprisms: perpendicular arrangements of (a) thinner and (b) thicker AgNPRs relative to the substrate; (c,d) tilted arrangements of AgNPR stacks; (e,f) perpendicular stack orientation. All scale bars are 50 nm.

Aqueous AgNPR dispersions have been used for the study of self-assembly, where nanoprisms were stabilized by a combination of a soluble thiol and citrate that was fully ionized at the high pH of the AgNPR synthesis. No sterically stabilizing agents, such as PVP, have been employed. Consequently, it can be postulated that electrostatic repulsions played a major role in long-range interactions that prevented random stacking and resulting disordered assemblies.[28] The main driving force of the ordering was entropically driven assembly, as documented in the reports on formation of colloidal mesophases.[27] For confined concentrated nanoparticle dispersions, organized structures are more favorable due to the total entropy gain from the close packing of the majority of the crowded particles that releases the solvent.[28,39] Typically, assemblies of AgNPRs have been prepared by drying concentrated dispersions, which is the most straightforward procedure. The AgNPR packing could be also achieved upon centrifugation that produced highly concentrated dispersions or upon natural sedimentation of the heavier nanoprisms. The description of the AgNPR self-assembled structures follows the progression of increase in AgNPR concentrations in dispersion and consequently increasing nanoparticle coverage on the substrate surface.

Side-by-Side AgNPR Stacking, Columnar Arrangements. Similar to discotic liquid crystals,[25,26] AgNPRs self-assemble in stacks of close-packed columnar structures (Figures 4–9), as it has been reported for different prismatic nanoparticles[23,25] including silver nanoprisms.[31] Stacking arrangements of nanoprisms are also favorable in the assembly driven by capillary forces.[40] Starting with relatively dilute dispersions, AgNPRs self-assemble into shorter fragments of the columns, with the sides of the

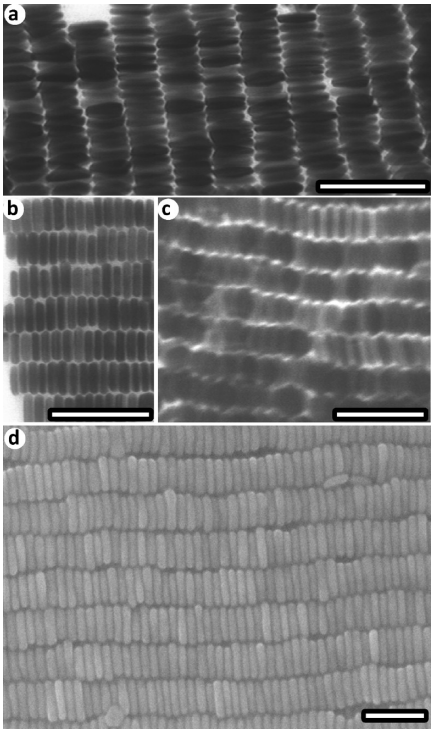

Figure 5. (a–c) TEM and (d) SEM images of columnar side-by-side stacking arrangements of self-assembled AgNPRs. All scale bars are 100 nm.

nanoprisms typically oriented perpendicular to the substrate, as illustrated in Figure 4a,b and has been previously reported for the assemblies of silver nanoprisms.[32] Tilted stacks could be also observed (Figure 4c,d). At higher nanoprism concentrations, the columns arrange closely together (Figure 5), maximizing an overall packing factor of the assemblies. The columnar stacks of nanoprisms typically align parallel to each other (Figures 5 and 6). Perpendicular arrangements of short stacks have also been observed both in the same plane on the substrate (Figure 4e) and in different layers (Figure 4f). Perpendicular arrangements likely arise from independent pinned growth of different columns and lead to more disordered assemblies overall.

The spacing between the stacked nanoprisms can be estimated to be 2.6 ± 0.3 nm. This spacing had been linked to the ligand layers that surround nanoparticles; for example, Chen and Carroll correlated the interparticle spacing to CTAB layers in their system.[12] Captopril size can be estimated as *ca.* 0.9 nm from molecular modeling. Captopril is a strongly binding thiol that is expected to coordinate tightly to the surface. The fact that the observed spacing is larger than the double layer of captopril can be attributed to the presence of other ligands, such as charge-stabilizing citrate as well as the electrostatic repulsion of carboxylate groups of both captopril and citrate at typical high values of pH in the system.

Columnar AgNPR Stacking, Tiling. The columnar packing of AgNPRs, shown in Figure 5, has been

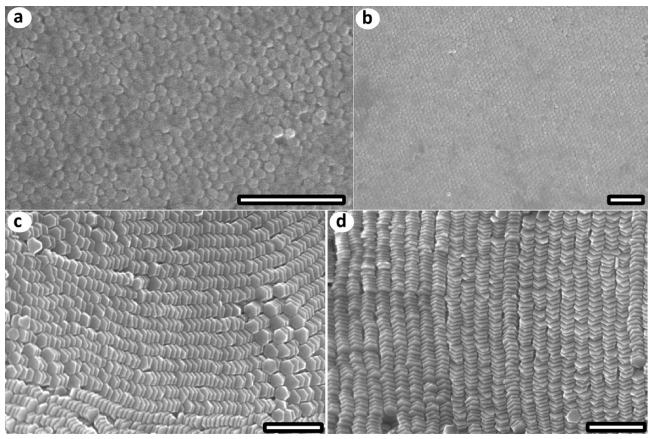

Figure 6. SEM images of (a,b) top view of tiling of AgNPR columnar arrangements; (c,d) tilted views of the assemblies. All scale bars are 300 nm.

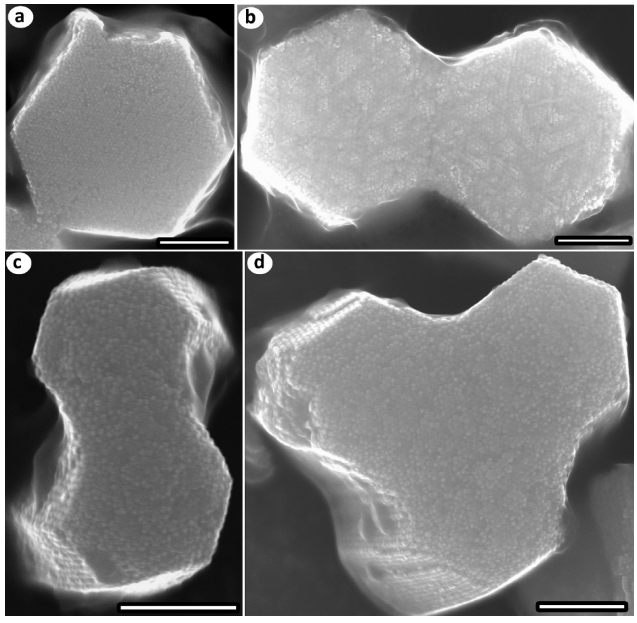

Figure 7. SEM images of top views of hexagonal morphologies of self-assembled AgNPR structures emerging upon slow drying of the dispersions. All scale bars are 500 nm.

formed at higher concentrations in the dispersions or higher surface coverage upon drying. Typically, there was a strong preference of columnar aggregates to maximize their contact with the surface and align perpendicular to the substrate (Figure 5b,d), while tilted assemblies (Figure 5a,c) have been observed less commonly. At even higher concentrations of nanoprisms, more massive assemblies have been formed. Due to their larger size, the interactions of these assemblies with the substrate become a less important factor, so these self-assembled structures arrange more randomly relative to the substrate and often with the faces of the prisms parallel to the surfaces. The surface of AgNPR assemblies then displays the patterns of the columnar arrangement, which is governed by the minimization of intercolumnar space (maximum exclusion of the solvent) and preservation of the symmetry of the hexagonal prisms as the structural building blocks of the assembly. The resulting packing is the hexagonal tiling displayed in Figure 6a,b. Tilted orientation of the AgNPR columnar stacking is shown in Figure 6c,d.

Morphologies of AgNPR Assemblies. Self-assembly of nanoparticles is similar in many aspects to molecular crystallization, where the symmetry of the molecules is often translated into crystal habits. The symmetry of the columnar packing of AgNPRs governs the morphologies of their self-assembled structures. The observed morphologies of the self-assembled AgNPRs preserve the hexagonal symmetry of AgNPRs or, more generally, C_3 symmetry of truncated triangular prisms. The self-assembled crystallites formed by AgNPRs were thus hexagonal prisms with the surface of the hexagons formed by the tiling of the nanoprisms and the columns running perpendicular to the surface

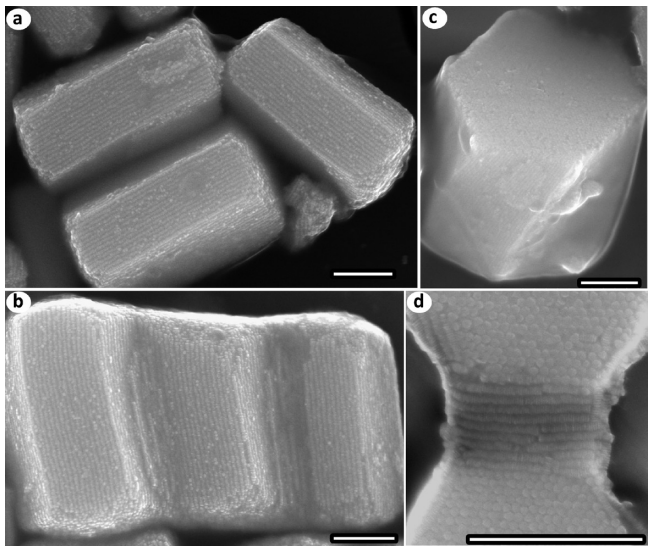

Figure 8. SEM images of (a,b) side views and (c) tilted views of the morphologies of self-assembled AgNPR structures; (d) shows a transitional area between two partially merged assemblies. All scale bars are 500 nm.

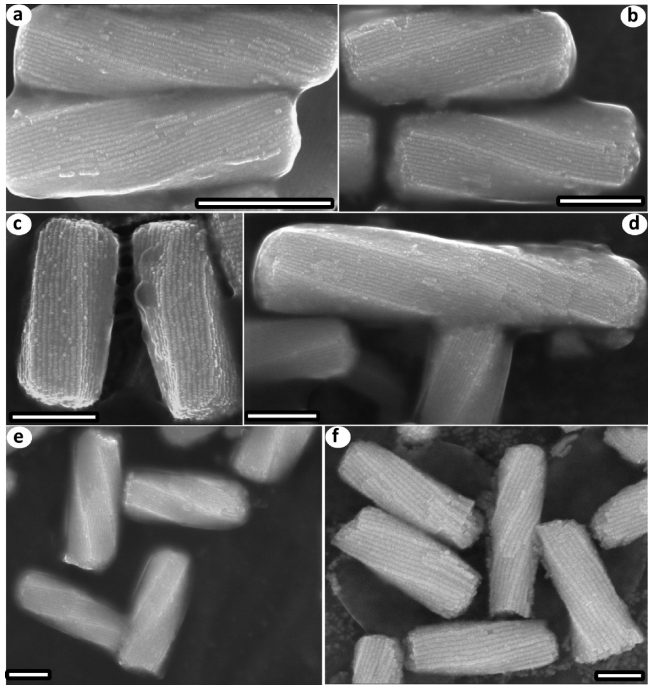

Figure 9. SEM images of different AgNPR samples displaying helical assemblies upon slow evaporation of their dispersions. All scale bars are 500 nm.

(Figure 7a,b). The lateral dimensions of these hexagonal crystals ranged from 0.8 to 1.5 μm. The side-view images of the self-assembled structures are shown in Figure 8a,b, and views at the tilt angles are presented in Figure 8c. The typical length of the AgNPR crystals along the columns varied from 1.2 to 2 μm. Thus, these self-assembled aggregates featured a fairly low anisotropy factor (length to diameter) of *ca.* 1.5. Intergrown crystallites were often observed (Figure 7c,d), some with a characteristic symmetric trefoil shape (Figure 7d) and characteristic transition zones of intergrown crystals (Figure 8d).

Long-Range Order and AgNPR Polydispersity. Defect-free AgNPR assemblies with the length span of several micrometers in size corroborate on a very good long-range order in the system. The key factor for the high degree of order in self-assembled structures is the low polydispersity of the synthesized AgNPRs. At the same time, an additional contributing factor is NP fractionation upon ordering. This fractionation is indicated by the common observation of impurities (NPs of different shape and size) on the surface of the self-assembled structures (*e.g.*, Figure 6a). The size

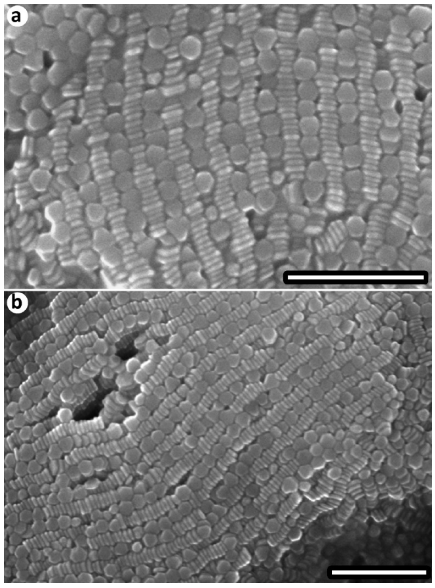

Figure 10. SEM images of alternating perpendicular AgNPR assemblies. All scale bars are 300 nm.

fractionation has been reported to be prominent for platelets[41] due to their appreciable area of contact in packed assemblies, which strongly favors a close contact of identical (or very similar in size) NPs. The resulting fractionation, which features a lot of similarity to how natural opals are formed, is responsible for the reported observation of ordered opal-like phases for platelets with appreciable polydispersity.[42]

Helical Assemblies. One of the most striking features of the AgNPR self-assembly that was observed in our system was helicity. Most of the assemblies featured well-defined twists in the packing of the columns (Figure 9) similar to chiral mesophases. The synthetic conditions for preparation AgNPRs forming helical assemblies are summarized in Table S1 (Supporting Information). The pitch of the helical twist was larger than the size of the aggregates and fairly constant at *ca.* 5−6 μm for well-defined helical structures (while a larger effective twist have been observed for less regular helical assemblies of smaller AgNPRs, as shown in Figure S11). Most observed variations of the twist could be attributed to nonperfect assemblies that were either merging with each other or disturbed by the substrate pinning. We have not observed any similar helical assemblies in our previous work with AgNPRs stabilized without chiral ligands.[38] Thus, the helicity likely originates from the chirality of the thiol ligand, captopril. The intermediates of the AgNPR synthesis, silver nanoclusters, are chiral, as it had been shown with the analogous monodisperse silver nanoclusters.[33,34] It is plausible that the chirality of the nanoclusters is imprinted onto the nanoprisms during nanocluster aggregation, and the chirality emerges in the helicity of the assemblies. At the same time, it is important to note that we have not been able to detect a significant chiro-optical response of our AgNPRs in the spectral range from 350 to 650 nm using circular dichroism spectroscopy,[43] in contrast with monodisperse silver nanoclusters stabilized with the captopril.[33,34] Such relatively weak imprinting of the chirality for the individual nanoprisms is likely responsible for a relatively large helical pitch of the assemblies of several micrometers. Both handedness of helices could be observed without preferential selection, as displayed in Figure 9c. Thus, the weak imprinting of the chirality in the individual prisms is the factor responsible for the lack of the chiral selectivity in the AgNPR helical assemblies and relatively large pitch of their helices. Investigating optical properties of the assemblies, such as circular dichroism,[44] can be worthwhile in future studies. Unfortunately, enantiomers of captopril are not commercially available, so we could not explore direct control of the helicity of the self-assembled AgNPR structures.

Other Types of AgNPR Assemblies. In several samples, an unusual perpendicular stacking of silver nanoprisms in assemblies has been observed (Figure 10). In some cases, a single layer of nanoprisms simply filled the grooves of the existing columnar arrays with the perpendicular orientation to the nanoprisms in the array. In other cases, within limited areas, perpendicular columnar stacking has been witnessed. While not perfect in order and limited in observed areas, the elements of these assemblies have been documented at least for three different nanoprism samples. All of these samples were similar in their relatively small nanoprism width (*ca.* 40 nm) and low aspect ratio of 5 (average thickness of 8 nm).

SERS Properties of AgNPRs. We have explored enhancement of the Raman scattering with the synthesized AgNPRs using a common thiol Raman probe, 5,5′-dithiobis(2-nitrobenzoic acid) (DTNBA) (Figure S9a). Important to note, no enhancement was detected both in solution and in dry state with the as-synthesized silver prisms. This observation can be reasonably explained by the presence of the strongly binding stabilizing thiol ligand on the surface of the prisms (that can be alternatively viewed as the formation of a passivating thiolate layer). Removal of the ligands (including the thiolate layer) could be successfully accomplished by the air plasma treatment using standard plasma cleaning instrumentation. Subsequently, both solid films and aqueous dispersions of AgNPR displayed enhancement of the Raman signal of the probe thiol molecule, DTNBA. After plasma treatment, the Raman spectra of DTNBA deposited on a solid films of AgNPRs (a monolayer to a bilayer average nanoparticle coverage, at the surface, as shown in Figure S7) on a quartz substrate are shown in Figure 11a. SEM images and UV−vis spectra characterizing size distribution and optical properties of the corresponding AgNPR samples are shown in Figure 11e,f, respectively. Raman

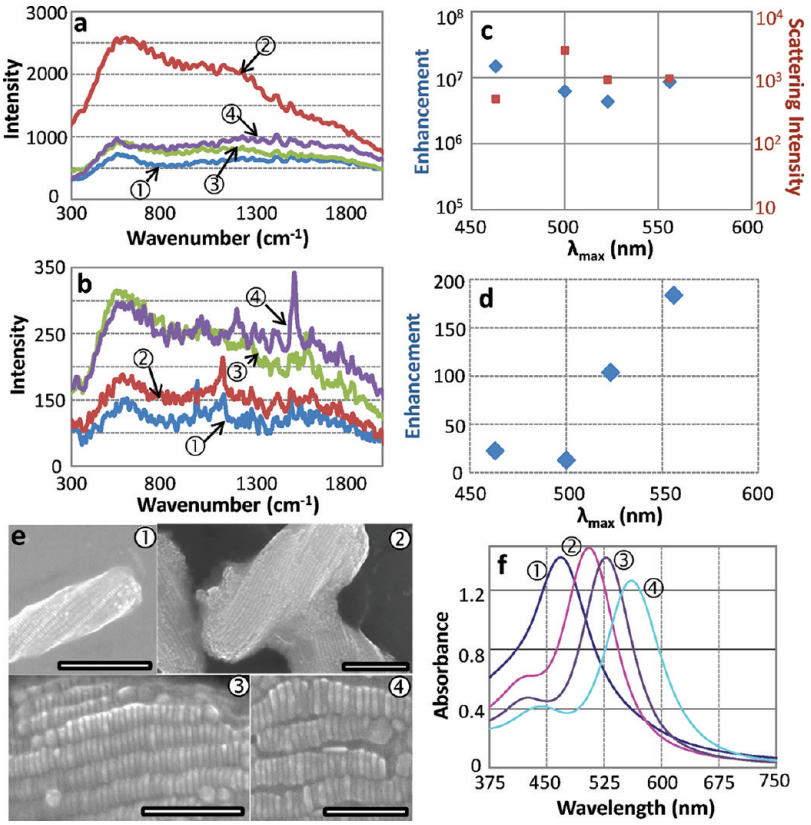

Figure 11. (a) Surface-enhanced Raman spectra (SERS) of 5,5′-dithiobis(2-nitrobenzoic acid) (DTNBA) deposited onto solid plasma-treated AgNPR films. Spectra were measured after deposition of ① 10 μL, ② 20 μL, ③ 5 μL, and ④ 10 μL of 10^{-9} M DTNBA, correspondingly. (b) SERS spectra of DTNBA in aqueous dispersions of plasma-treated AgNPRs (with twice lower concentration relative to as-synthesized) after deposition of ① 30 μL, ② 40 μL, ③ 10 μL, and ④ 10 μL 0.05 M DTNBA, respectively. (c) Bar graph displaying both relative enhancements of Raman signals measured by the ratio of peak intensities at 1520 cm^{-1} (left axis, blue points) and the intensity of the scattering by AgNPR at *ca.* 500 cm^{-1} (right axis, magenta points) for each solid AgNPR sample. (d) Comparison plot of λ_{max} for several AgNPR samples *vs* their SERS signal enhancement in dispersions. (e) SEM images showing dimensions of the respective AgNPRs samples used in SERS measurements (note that the representative SEM images of the solid films used for SERS measurements are shown in Figure S7b). Scale bars are ① 300 nm, ② 500 nm, ③ and ④ 200 nm. (f) UV−vis spectra of the respective AgNPRs samples used in SERS measurements.

spectra were actually measured from AgNPR samples dried on quartz slides, representative images of which films are shown in Figures S7 and S8. The main feature of the observed Raman signal from those solid films was the background inelastic scattering by AgNPRs in the solid state shown in Figure S9b. Similar scattering has also been observed with silver prisms prepared without thiol ligands[39] and thus is not related to possible fluorescence of thiolate species, which is typically observed at higher energies. Despite the strong scattering, an overall SERS enhancement by dry AgNPRs on the level of 10^7 (calculated for the DTNBA peak at 1520 cm^{-1}) could be realized, as shown in Figure 11c (together with the values of the scattering intensity). Larger enhancements in a solid state have been observed for smaller prisms, in which case the scattering was noticeably less.

After the oxidative plasma treatment, AgNPRs could be readily redispersed in water by pipetting high-purity water over the sample slides into a vial or by gentle sonication and SERS in dispersions could be measured. Importantly, there were no notable changes in AgNPR shape and integrity after plasma treatment and redispersion, as documented in Figure S9b,c. EDX analysis performed on the plasma-treated prisms (Figure S8) indicated complete removal of sulfur and chloride present in original samples. As well, no oxygen was detected in the plasma-treated AgNPR samples. Thus plasma treatment leaves the AgNPR morphology perfectly intact (as demonstrated in Figures S7 and S8) and removes thiolate ligands without formation of the detectable oxide layer. Spectra of prism samples before and after plasma treatment and redispersion are shown in Figure S10. The redispersed samples have broader peaks, so some AgNPR aggregation cannot be excluded though and the observed enhancement may not be solely attributed to single-particle SERS. An effective solution enhancement factor as large as 200 for larger AgNPRs could be realized, which is respectable considering averaging of the hotspots over *ca.* 0.2 cm^2 in the measurements. The largest enhancement in dispersions has been observed for the largest AgNPR used (Figure 11d,f), which can be reasonably

explained by a better overlap of their plasmonic resonance with the wavelength of the laser used at 785 nm.

Our future work will involve larger AgNPRs, where additional faceting can be induced by an excess of halide ions, which should be advantageous for SERS.

CONCLUSION

A novel synthetic procedure based on the controlled aggregation of nanoclusters has been discovered and optimized to reliably produce monodisperse aqueous thiol-stabilized silver nanoprisms with tunable thicknesses, lateral size, and plasmon resonances. The role of the reagents in the AgNPR synthesis has been investigated in detail; specifically, the central role of chloride for monodispersity and reproducibility, as well as the interplay of chloride and citrate, and chloride and a strong base have been discussed. Optical properties of the synthesized AgNPRs have been characterized. The bicolor AgNPR dispersion appearance has been attributed to the interplay of their sharp plasmonic resonances with the light scattering due to nanoprism thickness. By virtue of their monodispersity, the prepared AgNPRs self-assembled readily and displayed a rich variety of highly ordered patterns and morphologies of the assemblies with a long-range order of several micrometers. Notably, helical self-assembly patterns, attributed to the effect of the chiral thiol ligand, and alternating perpendicular column stacking have been observed. After oxidative removal of thiolate ligands, AgNPRs displayed SERS both in solid films and in solution. Future work is directed toward further exploration of the role of halides in the system, self-assembly of binary systems of silver nanoprisms of different sizes and aspect ratios and with other monodisperse nanoparticles, as well as studies of the optical properties of the AgNPR assemblies and their surface-enhanced Raman scattering.

EXPERIMENTAL SECTION

Reagents. Silver nitrate (99%), (2*S*)-1-[(2*S*)-2-methyl-3-sulfanylpropanoyl]pyrrolidine-2-carboxylic acid (captopril), hydrogen peroxide (99.999%), citric acid (Aldrich 99%), sodium borohydride (99%), potassium hydroxide pellets (99.99%), potassium chloride (analytical grade), and 5′5′-dithiobis(2-nitrobenzoic acid) (99%), all supplied by Aldrich, were used as received. High-purity deionized water (>18.3 MΩ·cm) was obtained using Millipore A10 Milli-Q.

Instrumentation. UV−vis spectra were acquired with either Ocean Optics QE-65000 fiber-optic UV−vis spectrometer or Cary 50Bio UV−vis spectrophotometer. Raman spectra were recorded using R-3000QE fiber-optic Raman spectrometer equipped with 290 mW laser at 785 nm (RSI). Electron microscopy (EM) imaging was done using Hitachi S-5200 with a carbon-coated Formvar grid (EMS Corp.). X-ray microanalysis has been measured using INCAx-sight (Oxford Instruments). Centrifugation was performed using either a VWR Clinical 200 or IEC Centra MP4 centrifuges. Organic ligand removal on dry samples has been done by a Harrick Plasma cleaner model PDC-32G.

Synthesis of Silver Nanoprisms. A typical silver nanoprism synthesis utilized a precursor solution of silver nanoclusters prepared similar to our previously reported work.[45,46] Reactions were performed in glass vials (20 mL, VWR) with total synthesis volumes ranging from 3 to 20 mL. A typical preparation of the monodisperse silver nanoprisms displaying well-defined self-assembly used the following reagents listed in order of their volumetric additions with their concentrations listed with the respective total molarity in the final solution listed in parentheses: in 1.9 mL of high purity water, 200 μL of 0.02 M citric acid (0.77 mM), 67 μL of 0.02 M captopril (0.26 mM), 500 μL of 0.005 M silver nitrate (0.48 mM), 250 μL of 0.2 M hydrogen peroxide (9.7 mM), 1750 μL of 0.001 M potassium chloride (0.34 mM), 120 μL of 0.1 M sodium borohydride (2.3 mM), and 380 μL of 0.1 M potassium hydroxide (7.4 mM) were added. Visually, the solution remained clear through the addition of the first five reagents. In some cases, a slight cloudiness was observed upon the addition of potassium chloride due to the formation of silver chloride. Upon reduction of silver ions with sodium borohydride, the cloudiness cleared, and the formation of crude nanoclusters was indicated by a color change: first to pale yellow, which then developed further to a deep brownish-red/orange color (Figure 1). Within 0.5 to 5 min after silver reduction, potassium hydroxide was added to promote the controlled aggregation of nanoclusters into nanoprisms. Upon KOH addition, the deep red/orange color faded (but not completely cleared, indicating the continuing presence of clusters/nanoparticles), and within 5−20 s, a bicolored appearance emerged first on the air−liquid interface and subsequently spread throughout the entire solution (the bicolored appearance arises due to the interplay of plasmon absorption and scattering and is indicative of larger metal nanoparticles,[47] thick silver nanoprisms in our case). The yield of the nanoclusters conversion to nanoprisms has been estimated by potentiometry to be 40−50% for the smaller nanoprisms and progressively higher for the larger ones (up to >90%), with the rest of the silver remaining largely in the form of silver thiolates due to the thiol excess used in the synthesis.

Preparation of Self-Assembled Nanoprisms. To prepare the samples for electron microscopy (EM) imaging and self-assembly, freshly synthesized dispersions were centrifuged in 15 mL centrifuge tubes twice for 20 min at 5000 rcf. After the first centrifugation, the supernatant was removed, leaving *ca.* 100 μL sample. The centrifuged sample was reconstituted to the original volume with water and centrifuged again. After the second centrifugation, the supernatant was removed near completely, leaving *ca.* 15 μL of the concentrated dispersion. The final silver concentration in these concentrated dispersions was *ca.* 0.07 M. These concentrated dispersions were deposited on a carbon-coated Formvar grid (EMS Corp.) to dry slowly, and their self-assembly was subsequently imaged by EM.

Measurements of Surface-Enhanced Raman Scattering (SERS). AgNPR samples were first concentrated by centrifugation, dispensed on a quartz slide, and dried in an oven at 65 °C for 1−2 min. The dry solid film of AgNPRs was then plasma-cleaned using a Harrick plasma cleaner at 0.5 Torr and highest power setting for 3 min. The surface coverage of the AgNPRs on the substrate was 0.508 μmol of silver per cm^2 that corresponded to approximately a monolayer coverage of the AgNPRs, as representatively shown in Figure S7. The integrity and the uniformity of the layer were monitored by optical microscopy. Important to mention that, for SERS experiments, AgNPRs were dried on a substrate fast, so they did not often form the helical assemblies (Figure S7). Since we have observed for this AgNPRs, as well as other silver nanoparticles, that close-packed structures are less active in SERS likely due to less interparticle spacing. For solid-state SERS measurements, dilute 5,5′-dithiobis(2-nitrobenzoic acid) solution in ethanol was dispensed onto the plasma-cleaned samples, dried, and then measured. For SERS measurements in prism dispersions (liquid phase), the plasma-cleaned

samples were redispersed into water by pipetting 1.0 mL of high-purity water over the quartz slide into a vial reconstituting AgNPR to half of their original, as-synthesized concentration. Occasionally, sonication was required for complete transfer of the plasma-cleaned AgNPR samples from the plasma-treated surfaces to aqueous dispersions. For SERS measurements, the dispersion of plasma-cleaned samples was combined in a quartz half-cell with 5,5′-dithiobis(2-nitrobenzoic acid) in THF.

Acknowledgment. The authors would like to thank NSERC and the Government of Ontario (ERA Award) for funding, Scott Smith for assistance with potentiometric measurements, Centre for Nanostructure Imaging, University of Toronto, for access to imaging facilities, Ilya Gourevich and Neil Coombs for the support with electron microscopy and valuable assistance with EDX measurements.

Supporting Information Available: Additional electron microscopy images and UV−vis spectra characterizing transient species, unfavorable synthetic conditions, and AgNPR treatment for SERS; Raman scattering and UV−vis data. This material is available free of charge *via* the Internet at http://pubs.acs.org.

REFERENCES AND NOTES

1. Xia, Y. Shape-Controlled Synthesis of Silver Nanoparticles for Plasmonic and Sensing Applications. *Plasmonics* **2009**, *4*, 171–179.
2. Burda, C.; Chen, X. B; Narayanan, R.; El-Sayed, M. A. The Chemistry and Properties of Nanocrystals of Different Shapes. *Chem. Rev.* **2005**, *105*, 1025–1102.
3. Giljohann, D. A.; Safaris, D. S.; Daniel, W. L.; Massich, M. D.; Patel, P. C.; Mirkin, C. A. Gold Nanoparticles for Biology and Medicine. *Angew. Chem., Int. Ed.* **2010**, *49*, 3280–3294.
4. Tao, A. R; Habas, S.; Yang, P. Shape Control of Colloidal Metal Nanocrystals. *Small* **2008**, *4*, 310–325.
5. Cobley, C. M.; Rycenga, M.; Zhou, F.; Li, Z.-Y.; Xia, Y. Etching and Growth: An Intertwined Pathway to Silver Nanocrystals with Exotic Shapes. *Angew. Chem., Int. Ed.* **2009**, *48*, 4824–4827.
6. Millstone, J. E.; Hurst, S. J.; Metraux, G. S.; Cutler, J. I.; Mirkin, C. A. Colloidal Gold and Silver Nanoparticles. *Small* **2009**, *5*, 646–664.
7. Wiley, B. J.; Im, S. H.; Li, Z. Y.; McLellan, J.; Siekkinen, A.; Xia, Y. Maneuvering the Surface Plasmon Resonance of Silver Nanostructures through Shape-Controlled Synthesis. *J. Phys. Chem. B* **2006**, *110*, 15666–15675.
8. Jin, R.; Cao, Y.; Hao, E.; Metraux, G. S.; Schatz, G. C.; Mirkin, C. A. Controlling Anisotropic Nanoparticle Growth through Plasmon Excitation. *Nature* **2003**, *425*, 487–490.
9. Xue, C.; Metraux, G. S.; Millstone, J. E.; Mirkin, C. A. Mechanistic Study of Photomediated Triangular Silver Nanoprism Growth. *J. Am. Chem. Soc.* **2008**, *130*, 8337–8344.
10. Metraux, G. S.; Mirkin, C. A. Rapid Thermal Synthesis of Silver Nanoprisms with Chemically Tailorable Thickness. *Adv. Mater.* **2005**, *17*, 412–415.
11. Zhang, Q.; Ge, J.; Pham, T.; Goebl, J.; Hu, Y.; Lu, Z.; Yin, Y. Reconstruction of Silver Nanoplates by UV Irradiation: Tailored Optical Properties and Enhanced Stability. *Angew. Chem., Int. Ed.* **2009**, *48*, 3516–3519.
12. Chen, S.; Carroll, D. L. Silver Nanoplates: Size Control in Two Dimensions and Formation Mechanisms. *J. Phys. Chem. B* **2004**, *108*, 5500–5506.
13. Hsu, M.-S.; Cao, Y.-W.; Wang, H.-W.; Pan, Y.-S.; Lee, B.-H.; Huang, C.-L. Time-Dependent Surface Plasmon Resonance Spectroscopy of Silver Nanoprisms in the Presence of Halide Ions. *Chem. Phys. Chem.* **2010**, *11*, 1742–1748.
14. Lee, B.-H.; Hsu, M.-S.; Hsu, Y.-C.; Lo, C.-W.; Huang, C.-L. A Facile Method To Obtain Highly Stable Silver Nanoplate Colloids with Desired Surface Plasmon Resonance Wavelengths. *J. Phys. Chem. C* **2010**, *114*, 6222–6227.
15. Lee, G. P.; Minett, A. I.; Innis, P. C.; Wallace, G. G. A New Twist: Controlled Shape-Shifting of Silver Nanoparticles from Prisms to Disks. *J. Mater. Chem.* **2009**, *19*, 8294–8298.
16. Zhang, J.; Langille, M. R.; Mirkin, C. A. Photomediated Synthesis of Silver Triangular Bipyramids and Prisms: The Effect of pH and BSPP. *J. Am. Chem. Soc.* **2010**, *132*, 12502–12510.
17. Lofton, C.; Sigmund, W. Mechanisms Controlling Crystal Habits of Gold and Silver Colloids. *Adv. Funct. Mater.* **2005**, *15*, 1197–1208.
18. Aherne, D.; Ledwith, D. M.; Gara, M.; Kelly, J. M. Optical Properties and Growth Aspects of Silver Nanoprisms Produced by a Highly Reproducible and Rapid Synthesis at Room Temperature. *Adv. Funct. Mater.* **2008**, *18*, 2005–2016.
19. Nie, Z.; Petukhova, A.; Kumacheva, E. Properties and Emerging Applications of Self-Assembled Structures Made from Inorganic Nanoparticles. *Nat. Nanotechnol.* **2010**, *5*, 15–25.
20. Markovich, G.; Collier, C. P.; Henrichs, S. E.; Ramacle, F.; Levine, R. D.; Heath, J. R. Architectonic Quantum Dots. *Acc. Chem. Res.* **1999**, *32*, 415–423.
21. Ming, T.; Kou, X.; Chen, H.; Wang, T.; Tam, H.-L.; Cheah, K. W.; Chen, J. Y.; Wang, J. Ordered Gold Nanostructure Assemblies Formed by Droplet Evaporation. *Angew. Chem., Int. Ed.* **2008**, *47*, 9685–9690.
22. Narayanan, S.; Wang, J.; Lin, X.-M. Dynamical Self-Assembly of Nanocrystal Superlattices during Colloidal Droplet Evaporation by *In Situ* Small Angle X-ray Scattering. *Phys. Rev. Lett.* **2004**, *93*, 135503–135506.
23. Talapin, D. V.; Shevchenko, E. V.; Bodnarchuk, M. I.; Ye, X.; Chen, J.; Murray, C. B. Quasicrystalline Order in Self-Assembled Binary Nanoparticle Superlattices. *Nature* **2009**, *461*, 964–967.
24. Gabriel, J.-C. P.; Davidson, P. New Trends in Colloidal Liquid Crystals Based on Mineral Moieties. *Adv. Mater.* **2000**, *12*, 9–20.
25. Saunders, A. E.; Ghezelbash, A.; Smilgies, D.-M.; Sigman, M. B., Jr.; Korgel, B. Columnar Assembly of Colloidal Nanodisks. *Nano Lett.* **2006**, *6*, 2959–2963.
26. Boyd, B. J.; Rizwan, S. B.; Dong, Y.-D.; Hook, S.; Rades, T. Self-Assembled Geometric Liquid Crystalline Nanoparticles Imaged in Three Dimensions: Hexosomes Are Not Necessarily Flat Hexagonal Prisms. *Langmuir* **2007**, *23*, 12461–12464.
27. Mourad, M. C. D.; Petukhov, A. V.; Vroege, G. J.; Lekkerkerker, H. N. W. Lyotropic Hexagonal Columnar Liquid Crystals of Large Colloidal Gibbsite Platelets. *Langmuir* **2010**, *26*, 14182–14187.
28. Kleshchanok, D.; Petukhov, A. V.; Holmqvist, P.; Byelov, D. V.; Lekkerkerker, H. N. W. Structures and Phase Behavior in Mixtures of Charged Colloidal Spheres and Platelets. *Langmuir* **2010**, *26*, 13614–13621.
29. Onsager, L. The Effects of Shape on the Interaction of Colloidal Particles. *Ann. N.Y. Acad. Sci.* **1949**, *51*, 627–659.
30. Grzybowski, B. A.; Wilmer, C. E.; Kim, J.; Browne, K. P.; Bishop, K. J. M. Self Assembly: From Crystals to Cells. *Soft Matter* **2009**, *5*, 1110–1128.
31. Yamada, M.; Shen, Z.; Miyaki, M. Self-Assembly of Discotic Liquid Crystalline Molecule-Modified Gold Nanoparticles: Control of 1D and Hexagonal Ordering Induced by Solvent Polarity. *Chem. Commun.* **2006**, *24*, 2569–2571.
32. Chen, S.; Carroll, D. L. Synthesis and Characterization of Truncated Triangular Silver Nanoplates. *Nano Lett.* **2002**, *2*, 1003–1007.
33. Xue, C.; Li, Z.; Mirkin, C. A. Large-Scale Assembly of Single-Crystal Silver Nanoprism Monolayers. *Small* **2005**, *1*, 513–516.
34. Bae, Y.; Kim, N. H.; Kim, M.; Lee, K. Y.; Han, S. W. Anisotropic Assembly of Ag Nanoprisms. *J. Am. Chem. Soc.* **2008**, *130*, 5432–5433.
35. Henglein, A.; Giersig, M. Formation of Colloidal Silver Nanoparticles: Capping Action of Citrate. *J. Phys. Chem. B* **1999**, *103*, 9533–9539.
36. Walter, M.; Akola, J.; Acevedo, O. L.; Jadzinsky, P. D.; Calero, G.; Ackerson, C. J.; Whetten, R. L.; Gronbeck, H.; Hakkinen, H. A Unified View of Ligand-Protected Gold Clusters as Superatom Complexes. *Proc. Natl. Acad. Sci. U.S.A.* **2008**, *105*, 9157–9162.

37. Linnert, T.; Mulvaney, P.; Henglein, A.; Weller, H. Long-Lived Nonmetallic Silver Clusters in Aqueous Solution: Preparation and Photolysis. *J. Am. Chem. Soc.* **1990**, *112*, 4657–4664.
38. Cathcart, N.; Frank, A. J.; Kitaev, V. Silver Nanoparticles with Planar Twinned Defects: Effect of Halides for Precise Tuning of Plasmon Resonance Maxima from 400 to >900 nm. *Chem. Commun.* **2009**, *46*, 7170–7172.
39. Purdy, K. R.; Fraden, S. Influence of Charge and Flexibility on Smectic Phase Formation in Filamentous Virus Suspensions. *Phys. Rev. E* **2007**, *76*, 011705-1–011705-8.
40. Dimitrov, A. S.; Nagayama, K. Continuous Convective Assembling of Fine Particles into Two Dimensional Arrays on Solid Surfaces. *Langmuir* **1996**, *12*, 1303–1311.
41. Byelov, D. V.; Mourad, M. C. D.; Snigireva, I.; Snigirev, A.; Petukhov, A. V.; Lekkerkerker, H. N. W. Experimental Observation of Fractionated Crystallization in Polydisperse Platelike Colloids. *Langmuir* **2010**, *26*, 6898–6901.
42. Van der Beek, D.; Radstake, P. B.; Petukhov, A. V.; Lekkerkerker, H. N. W. Fast Formation of Opal-like Columnar Colloidal Crystals. *Langmuir* **2007**, *23*, 11343–11346.
43. Govorov, A. O. Plasmon-Induced Circular Dichroism of a Chiral Molecule in the Vicinity of Metal Nanocrystals. Application to Various Geometries. *J. Phys. Chem. C* **2011**, *115*, 7914–7923.
44. Fan, Z.; Govorov, A. O. Helical Metal Nanoparticle Assemblies with Defects: Plasmonic Chirality and Circular Dichroism. *J. Phys. Chem. C* **2011**, *115*, 13254–13261.
45. Cathcart, N.; Mistry, P.; Makra, C.; Pietrobon, B.; Coombs, N.; Jelokhani-Niaraki, M.; Kitaev, V. Chiral Thiol-Stabilized Silver Nanoclusters with Well-Resolved Optical Transitions Synthesized by a Facile Etching Procedure in Aqueous Solution. *Langmuir* **2009**, *25*, 5840–5846.
46. Cathcart, N.; Kitaev, V. Silver Nanoclusters: Single-Stage Scaleable Synthesis of Monodisperse Species and Their Chirooptical Properties. *J. Phys. Chem. C* **2010**, *114*, 16010–16017.
47. Xia, Y.; Xiong, Y. J.; Lim, B.; Skrabalak, S. E. Shape-Controlled Synthesis of Metal Nanocrystals: Simple Chemistry Meets Complex Physics? *Angew. Chem., Int. Ed.* **2009**, *48*, 60–103.